CrystEngComm

Accepted Manuscript

ROYAL SOCIETY OF CHEMISTRY

www.rsc.org/crystengcomm

Self-Assemble SnO_2@TiO_2 Porous Nanowire-Nanosheet Heterostructures for Enhanced Photocatalytic Property

Banghong Zhou,[1] Shuanglei Yang,[1] Wei Wu,[2] Lingling Sun,[3] Mei Lei,[3] Jun Pan[1,] and Xiang Xiong[1,*]*

[1] State Key Laboratory for Powder Metallurgy, Central South University, Changsha 410083, P. R. China,

[2] Laboratory of Functional Nanomaterials and Printing Electronics, School of Printing and Packaging, Wuhan University, Wuhan 430072, P. R. China,

[3] Key Laboratory of Artificial Micro- and Nano-structures of Ministry of Education, School of Physics and Technology, Wuhan University, Wuhan 430072, P. R. China

*To whom correspondence should be addressed: xiongx@csu.edu.cn or jun.pan@csu.edu.cn

Abstract

One-dimension semiconductor heterostructures with unique properties are suited to the application in photocatalysis field. In this study, rational designed SnO_2@TiO_2 porous nanowire-nanosheet heterostructures were realized by a facile hydrothermal method via loading TiO_2 nanosheets onto SnO_2 porous nanowires. One-dimension porous heterostructures formed via the self-assembly process. Due to the improved photon absorption ability and more active sites, the special heterostructures showed enhanced photocatalytic property under mixed light, nearly 2.5 times faster than that of SnO_2 porous nanowires. Our results suggest that the SnO_2@TiO_2 porous nanowire-nanosheet heterostructures were considered for promising photocatalyst.

Keywords: Tin dioxide, titanium dioxide, heterojunction, photocatalytic activity.

Introduction:

As a representative and the most widely used semiconductor photocatalyst, titanium dioxide (TiO_2) has received more interests due to its strong UV light absorption, powerful oxidation property, nontoxicity and excellent photostability.[1-5] However, the photocatalytic performance of TiO_2 is encountered by two intrinsic drawbacks, the first one is the relatively wide band gap (~ 3.2 eV), which limits its application to visible region, the other is the fast recombination of photo-generated electron/hole (e^-/h^+), which reduces the quantum efficiency of photo-induced redox reaction. Therefore, the study on how to improve the absorptivity in the visible region and the quantum efficiency of TiO_2 attracts more attentions.

In order to overcome these drawbacks, several strategies have been developed in the previous studies. Such as changing the morphology and phase of TiO_2,[2, 6-8] loading the noble metal nanoparticles on the surface of TiO_2,[9-11] constructing the semiconductor/TiO_2 heterostructures[12-15]. Particularly, constructing heterostructures is an effective and feasible method because of the special band alignment could improve the photon absorption[16] and promote the separation of the electron/hole pairs.[17] Recent years, various semiconductor heterostructures based on TiO_2 have been developed, such as SnO_2/TiO_2,[18-20] Fe_2O_3/TiO_2,[21, 22] CdS/TiO_2,[15, 23] Fe_3O_4/TiO_2,[24] Cu_2O/TiO_2[25] .

Using 1D photocatalysts could overcome the drawbacks simultaneously as these special structures provide a continuous long carrier transfer path as compared with nanoparticles. Meanwhile, 1D photocatalysts can be separated and recycled easily because of their large length to diameter ratio.[26, 27] Among the many varieties of 1D nanostructures, porous nanowires are particularly interesting, not only for the unique porous structural and physical chemical properties

relative to their bulk counterparts, but also for their outstanding performance in optic and electronic fields.[28] Furthermore, it has been proven that the porous structure effectively promotes the direct growth of secondary nanostructures due to their porous surface and large surface area.[29] Moreover, the synergistic effect between two structures could improve the photocatalytic performance efficiently.[27] Hence, 1D porous SnO_2 nanowires were used as the framework to direct growth the TiO_2 nanosheets.

Based on the above discussion, we rationally designed the SnO_2@TiO_2 porous nanowire-nanosheet heterostructures by a self-assembly process. The proposed photodegradation mechanism of the SnO_2@TiO_2 heterostructures was shown in **Scheme 1**.The growth mechanism of the heterostractures, which combines with porous nanowires and nanosheets, was systematically studied. Furthermore, the morphology evolution and photocatalytic properties of SnO_2@TiO_2 heterostructures were also deeply investigated.

Experimental Sections

Materials Synthesis

Synthesis of porous SnO_2 nanowires

Porous SnO_2 nanowires (SnO_2 NWs) were fabricated according to a modified method.[30] Briefly, 3.5 g oxalic acid dehydrate (Sinopharm Chemical Reagent Co., AR) was dispersed completely in 5 mL absolute ethanol, then 50 mL polyethylene glycol-400 (PEG400, Sinopharm Chemical Reagent Co.) was added under vigorous stirring. After several minutes stirring, a certain amount of $SnCl_2{\cdot}2H_2O$ (Guangdong Guanghua Sci-Tech Co., AR) mixed within ethylene glycol (EG, Sinopharm Chemical Reagent Co.) was added to the above solution, and continuously stirred for

another 15 mins. When the $SnCl_2 \cdot 2H_2O$ was dissolved completely, 10 mL deionized water was dropwise added into the solution, yielding a white suspension immediately. After stirring for another half an hour, the as-prepared precipitation (SnC_2O_4 precursor) was separated by centrifugation, washed several times alternately with absolute ethanol and deionized water and dried in vacuum oven at 90 ˚C. Then the as-prepared SnC_2O_4 precursor was calcined at 650 ˚C for 3 h under air to obtained porous SnO_2 nanowires.

Synthesis of SnO_2@TiO_2 porous nanowire-nanosheet heterostructures

SnO_2@TiO_2 porous nanowire-nanosheet heterostructures were synthesized by a hydrothermal method.[31] Firstly, a certain amount of as-obtained SnO_2 NWs was dispersed into 50 mL absolute ethanol under ultrasonic, then 0.5 mL Diethylenetriamine (DETA, Aladdin Industrial Co., AR) was added under stirring. Several minutes late, 2 mL tetrabutyl titanate ($Ti(O^tBu)_4$, Aladdin Industrial Co., AR) was injected into the solution. To deposit TiO_2 nanosheets on SnO_2 nanowires, the solution was transferred into a 100 mL Teflon-lined stainless steel autoclave, followed by heating at 200 ˚C for 20 h in an electric oven. After heating, the autoclave was cooled naturally to room temperature. The light yellow precipitate was separated and washed with deionized water several times by centrifugation, then dried at 110 ˚C in vacuum oven overnight.

Characterization

The transmission electron microscopy (TEM) images and high-resolution transmission electron microscopy (HRTEM) analysis were performed with a JEOL JEM-2100F. The scanning electron microscopy (SEM) images were obtained by using a high resolution field emission SEM (FEI Nova-400). Powder X-ray diffraction (XRD) patterns of the samples were collected using a D/ruax2550PC (Japan, Cu K_α radiation (λ = 0.1542 nm) under a scan rate of 5° 2θ S^{-1}. The specific

surface area of the samples was measured using a BET analyzer (ASAP 2020M) at 77 K.

Photocatalytic Tests

The photocatalytic activities of the as-prepared samples (pure SnO_2 nanowires and SnO_2@TiO_2 heterostructures) were studied by photodegrading rhodamine B (RhB) in simulated wastewater. In the photocatalytic experiments under mixed light, 5 mg of the products were re-dispersed in 10 mL of the RhB solution (10 mg·L^{-1}) . Prior to illumination, the mixed solution was stored for 30 mins in the dark with magnetic stirring to achieve adsorption/desorption equilibrium. Then, a mercury lamp (300 W) was used to illuminate the solutions. The reaction solutions were withdrawn from the reactor at 15 mins illumination intervals and centrifuged to separate the photocatalyst. After that, to monitor the progress of the degradation of RhB, the corresponding UV-visible spectra (measured in the range of 450 to 650 nm, the maximum absorption wavelength of RhB is about 550 nm.) were recorded by a Shimadzu 2550 UV-visible spectrophotometer (as a control, 10 mg·L^{-1} RhB was subjected to the same illumination without photocatalyst). The mixed light source came from a mercury lamp of BL-GHX-V apparatus.

Results and discussion

The hydrothermal method has been widely used for the synthesis of TiO_2 nanostructures.[32-34] In this work, TiO_2 nanosheets have been self-assembled on the porous SnO_2 nanowires with the hydrothermal method by the solution of $Ti(O^tBu)_4$, DETA and absolute ethanol.

The synthetic process is illustrated in **Scheme 2**. Firstly, porous SnO_2 nanowires were prefabricated by calcining the SnC_2O_4 precursor in the air. Then, the TiO_2 nanosheets self-assemble directly on the porous SnO_2 nanowires, formed SnO_2@TiO_2 porous nanowire-nanosheet

heterostructures. After being calcined at 500 ˚C in air, the highly crystalline SnO_2@TiO_2 porous nanowire-nanosheet heterostructures were successfully obtained. **Fig. 1** shows the SEM and TEM images of the SnC_2O_4 precursor, the porous SnO_2 nanowires and the SnO_2@TiO_2 heterostructures. It can be seen that the SnC_2O_4 precursor is about 100 nm in diameter, and has smooth surface (**Fig. 1a**). The morphology of the SnO_2 porous nanowires doesn't change tremendously and many holes can be obviously seen, as shown in **Fig. 1b**. From the SEM image (**Fig. 1c**) and TEM image (**Fig. 1d**) of the SnO_2@TiO_2 porous nanowire-nanosheet heterostructures, it revealed that the porous structure and the diameter of the SnO_2 nanowires also doesn't change during the hydrothermal process. Prior to the calcined treatment, the length of the TiO_2 nanosheets is about 50 nm (**Fig. 1d**). Selected area electron diffraction (SEAD) patterns insets in **Fig. 1b** and **Fig. 1d** reveals that SnO_2 nanowires and TiO_2 nanosheets are crystalline. After being calcined, TiO_2 nanosheets with a length of about 50 nm are identified which are slightly recrystallized due to curly tail (**Fig. 1e**). **Fig. 1f** shows the High-resolution TEM image of the SnO_2@TiO_2 porous nanowire-nanosheet heterostructures after being calcined**.** As is shown, clear lattice fringes can be observed. The spacing of the crystallographic planes are 0.264 nm and 0.335 nm, respectively, corresponding to the (101) and (110) planes of the rutile-structured SnO_2 crystal, which suggest that SnO_2 nanowires have no preferred growth orientation. Moreover, lattice fringes of TiO_2 nanosheets are measured to be 0.167 nm and 0.352 nm, corresponding to the (211) and (101) planes of anatase crystal structure TiO_2, respectively. To make sure that fringes are real atomic planes but Moire fringes, another clearer HRTEM image was shown in **Fig. S2**. These results reveal that the SnO_2@TiO_2 porous nanowire-nanosheet heterostructures were successfully fabricated in this work.

The growth mechanism of the SnO_2@TiO_2 porous nanowire-nanosheet heterostructures was clearly revealed from the **Fig. 2**. At the beginning of self-assemble process, nucleation occurs at the

grain boundary of SnO_2 since the alcoholysis of $Ti(O^tBu)_4$ (**Fig. 2a**). With the time prolonging, hydrated titanium oxides grow slowly (**Fig. 2b, 2c**). 16 hours later, the length of the TiO_2 nanosheets is about 30 nm. After being reacted 24 h, the length of the TiO_2 nanosheets increases to about 50 nm (**Fig. 2d**). **Fig. 3** shows the morphology of the SnO_2@TiO_2 porous heterostructures without (**Fig. 3a**) or with (**Fig. 3b**) assisted catalyst DETA. Firstly and most important, the TiO_2 nanosheets self-assemble onto the SnO_2 porous nanowires because of the DETA, which catalyze the alcoholysis of $Ti(O^tBu)_4$ to form TiO_2 nanosheets and assist the self-assembly of the as-formed TiO_2 nanosheets through electrostatic interactions[27, 35] and stereo-hindrance effect.[36] Secondly, the hydrated titanium oxides prefer to grow independently rather than form a continuous coated layer may attribute to lattice compatibility.[37, 38] To see the calcining treatment influences the morphology of SnO_2@TiO_2. The heterostructures were calcined at 500 ˚C for 2 h in the air

The chemical composition of the different samples was characterized by X-ray diffraction. **Fig. 4** shows the XRD patterns of the as-prepared SnO_2 nanowires and the SnO_2@TiO_2 porous nanowire-nanosheet heterostructures before and after calcining treatment. The all peaks corresponding to both TiO_2 and SnO_2, which can be assigned to rutile SnO_2 (JCPDS card No.41-1445) and anatase TiO_2 (JCPDS card no. 21-1272), respectively. Furthermore, after being calcined at 500 ˚C in air for 2 h, the degree of crystallinity of the as-prepared SnO_2@TiO_2 heterostructures increased immensely. Particularly, the peak (101) of TiO_2 nanosheets was obtained due to the calcining treatment.

Fig. 5 shows the UV-Vis optical absorption spectra. SnO_2 porous nanowires show a gradually increasing curve with no obvious absorption edge, which corresponds to the special porous structure of SnO_2 nanowires. The porous structure improves the photon absorption efficiency during the

visible light region. On the contrary, SnO_2@TiO_2 porous nanowire-nanosheet heterostructures show an obvious red shift of ca. 50 ~ 70 nm. The SnO_2@TiO_2 porous nanowire-nanosheet heterostructures show considerable increase of absorption in the spectrum regime of 330 ~ 700 nm, compared to pure SnO_2 porous nanowires. This enhancement of the light harvesting is mainly attributed to the TiO_2 nanosheets coating layer.

Fig. 6 shows the degradation profiles of the RhB under mixed light (UV and Visible light) with different photocatalysts. After being exposed to light for a specific time, the remaining RhB concentration (%) was estimated by the following equation:

$$\%RhB\ concentration = I_t/I_0 \times 100\ \%$$

where I_t is the intensity of the characteristic peak of RhB at the illumination time t min and I_0 is the initial intensity (that is, after the dark adsorption equilibrium, t = 0 min). **Fig. 6a, b** shows the UV-Vis spectra evolution of RhB. Among the two as-prepared samples, the pseudo first-order equation was adopted to describe the experimental data due to the very low initial concentrations of the substrates as follows:

$$-ln(C/C_0) = kt$$

where *k* is a reaction rate constant. As is shown in **Fig. 6c**, the order of the k values, which is derived from the plots of $-ln(C/C_0)$ versus irradiation time (*t*), is summarized as follows: the reaction rate constant of SnO_2@TiO_2 heterostructures is 2.5 times larger than the SnO_2 porous nanowires. This result is in good agreement with our goals: to improve the photocatalytic efficiency, we assemble the structure of the heterostructure that rutile SnO_2 nanowires loaded with anatase TiO_2 to form many interfaces which are similar to the P25. The results demonstrated that the SnO_2@TiO_2

heterostructures obtained in this work possess excellent properties in photodegradation reactions. The contrast shows that RhB self-degraded slowly (**Fig. 6d**) when it was exposed to mixed light. So, the photodegradation process of the RhB can be mainly attributed to the SnO_2@TiO_2 photocatalysts. As is shown, the degradation of RhB by the pure SnO_2 porous nanowires is less significant than the other catalysts, and only 78.7 % of RhB was degraded after being illuminated for 90 min. On the one hand, pure SnO_2 porous nanowires has low excitation efficiency of e^-/h^+ pairs due to the wide band gap (~ 3.6 eV) of SnO_2, which leads to a limited absorption of photons; On the other hand, pure SnO_2 porous nanowires has low quantum efficiency because of the recombination of photo-generated electron/hole (e^-/h^+) pairs. Compare to pure SnO_2, the SnO_2@TiO_2 porous nanowire-nanosheet heterostructures exhibit higher photocatalytic activity, with a degradation rate of 98.1 % for RhB, respectively. The improved photocatalytic activity can be assigned to the contribution of the synergistic effect of SnO_2 (rutile phase) and TiO_2 (anatase phase). The TiO_2 sheets with narrow band gap (~ 3.2 eV) enhance the photon absorption and the SnO_2 nanowires provides continuous path for the faster transfer of carrier.

The reasons for the high photocatalytic performance of SnO_2@TiO_2 porous nanowire-nanosheet heterostructures could be explained in details as follows: (I) As a advantage of nano-materials, the larger specific surface areas (~ 47 m^2/g, see **Fig. S1**) offer more active sites and absorb more photons, which leads to a higher photocatalytic performance.[19, 39] (II) Considering the band alignment between SnO_2 and probability within both SnO_2 and TiO_2, the band alignment between SnO_2 and TiO_2 is generally classified as a type II structure (staggered band alignment between these two different materials). In this band-gap configuration, when photogenerated e^-/h^+ pairs are generated in SnO_2 nanowires and TiO_2 nanosheets, the electrons on the TiO_2 sheets surface transfer swiftly to the conduction band of SnO_2 via interfaces; similarly, the holes on the SnO_2 surface migrate to TiO_2

owing to the different valence band edge[19, 39, 40]. (III) As an advantage of our synthetic method, the TiO_2 nanosheets grow directly on the surface of SnO_2 porous nanowires, which improves the negative charge injection from TiO_2 to SnO_2 and promotes the separation of hole-electron pairs at the interface.[41] Moreover, the one-dimensional long structure of SnO_2 porous nanowires promote charge transfer;[42] the high porosity and large surface area of the SnO_2@TiO_2 enhance the mass transfer of RhB and the independence of TiO_2 nanosheets impede the recombination of photo-generated electrons and holes at the same time[43]. Moreover, the nanosheets/nanowires-type structure possesses a large interfacial region, owing much structure defects, which can improve the charge carrier separation to a great degree.[44, 45] (IV) The TiO_2@SnO_2 heterostructures improve the photon utilization efficiency due to their special structure shown in **Fig. 5.** The TiO_2@SnO_2 heterostructures has an obvious red shift of ca. 50 ~ 70 nm in the absorption edge, compared with the pure SnO_2 nanowires. This larger absorption edge would lead to the enhancement of the photocatalytic performance of the SnO_2@TiO_2 heterostructures.[46, 47] When conventional TiO_2@SnO_2 (sosoloid or core/shell) heterostructures was irradiated with mixed light, part of the incident photons were directly absorbed by SnO_2 and TiO_2, the others were reflected and scattered by SnO_2 nanowires or TiO_2 nanosheets. As to porous TiO_2@SnO_2 porous nanowire-nanosheet heterostructures, the photon-matter interaction rates increased vastly because of the effective optical path length was increased due to the special porous structure,[48, 49] which leading to a higher light harvesting based on the Beer-Lambert Law. (V) The SnO_2@TiO_2 heterostructures has a special interface structure that was similar to P25, which offer lots of highly distorted, tetrahedral Ti^{4+} sites at the interface of rutile SnO_2 nanowires and anatase TiO_2 nanosheets. These tetrahedral Ti^{4+} sites own higher photocatalytic activity than conventional Ti^{4+} sites.[50]

Conclusions

In summary, rationally designed SnO_2@TiO_2 porous nanowire-nanosheet heterostructures have been successfully synthesized through a self-assembly process. In the presence of DETA, TiO_2 formed through the alcoholysis of $Ti(O^tBu)_4$, and then self-assemble to form SnO_2@TiO_2 porous nanowire-nanosheet heterostructures . In comparison with the uncoated porous SnO_2 nanowires, the SnO_2@TiO_2 heterostructures exhibited the better photocatalytic performance，more than nearly 2.5 times faster，than that of SnO_2 porous nanowires for the photodegradation of RhB. In particular, SnO_2@TiO_2 heterostructures processed several excellent properties including a continuous carrier transfer path for fast transfering carrier, suitable band engineering for charge carriers separation, interface for supplying abundant active sites and unique heterostructures for resistance to photo induced electron/hole pairs agglomeration. We assumed that the synergistic effects of the aforementioned factors contributed to the enhanced photocatalytic performance of the SnO_2@TiO_2 heterostructures.

Acknowledgment

We gratefully acknowledge financial support by the National Science Foundation of China (51302325), Program for New Century Excellent Talents in University (NECT-2012-003), the Scientific Research Foundation for the Returned Oversea China Scholars, the Hunan Youth Innovation Platform and Program for Shenghua Overseas Talent (1681-7601110203) from Central South University (CSU).

Notes

The authors declare no competing financial interest.

References

1. Chen, D. W. and A. K. Ray. *Applied Catalysis B-Environmental*, 1999. **23**: p. 143-157.

2. Macak, J. M., M. Zlamal, J. Krysa and P. Schmuki. *Small*, 2007. **3**: p. 300-304.

3. Testino, A., I. R. Bellobono, V. Buscaglia, C. Canevali, M. D'Arienzo, S. Polizzi, R. Scotti and F. Morazzoni. *Journal of the American Chemical Society*, 2007. **129**: p. 3564-3575.

4. Fujishima, A., X. T. Zhang and D. A. Tryk. *Surface Science Reports*, 2008. **63**: p. 515-582.

5. Tian, G. H., H. G. Fu, L. Q. Jing, B. F. Xin and K. Pan. *Journal of Physical Chemistry C*, 2008. **112**: p. 3083-3089.

6. Boppella, R., P. Basak and S. V. Manorama. *ACS Applied Materials Interfaces*, 2012. **4**: p. 1239-1246.

7. Zheng, X., Q. Kuang, K. Yan, Y. Qiu, J. Qiu and S. Yang. *ACS Applied Materials Interfaces*, 2013. **5**: p. 11249-11257.

8. Wu, H. B., H. H. Hng and X. W. Lou. *Advanced Materials*, 2012. **24**: p. 2567-2571.

9. Yu, D. H., X. Yu, C. Wang, X. C. Liu and Y. Xing. *ACS Applied Materials Interfaces*, 2012. **4**: p. 2781-2787.

10. Wu, W., L. Liao, S. Zhang, J. Zhou, X. Xiao, F. Ren, L. Sun, Z. Dai and C. Jiang. *Nanoscale*, 2013. **5**: p. 5628-5636.

11. Lee, J. and W. Choi. *Journal of Physical Chemistry B*, 2005. **109**: p. 7399-7406.

12. Xiao, F. X. *ACS Applied Materials Interfaces*, 2012. **4**: p. 7055-7063.

13. Liu, Z., D. D. Sun, P. Guo and J. O. Leckie. *Nano Letter*, 2007. **7**: p. 1081-1085.

14. Chalasani, R. and S. Vasudevan. *ACS Nano*, 2013. **7**: p. 4093-4104.

15. Pan, J., J. Li, Z. Yan, B. Zhou, H. Wu and X. Xiong. *Nanoscale*, 2013. **5**: p. 3022-3029.

16. Lin, Y., S. Zhou, X. Liu, S. Sheehan and D. Wang. *Journal of the American Chemical Society*, 2009. **131**: p. 2772-2773.

17. Cao, T., Y. Li, C. Wang, C. Shao and Y. Liu. *Langmuir*, 2011. **27**: p. 2946-2952.

18. Pan, J., S. M. Huhne, H. Shen, L. S. Xiao, P. Born, W. Mader and S. Mathur. *Journal of Physical Chemistry C*, 2011. **115**: p. 17265-17269.

19.Cao, Y., X. T. Zhang, W. S. Yang, H. Du, Y. B. Bai, T. J. Li and J. N. Yao. *Chemistry of Materials*, 2000. **12**: p. 3445-3448.

20. Wang, C., C. Shao, X. Zhang and Y. Liu. *Inorganic Chemistry*, 2009. **48**: p. 7261-7268.

21. Sun, L., W. Wu, S. Yang, J. Zhou, M. Hong, X. Xiao, F. Ren and C. Jiang. *ACS Applied Materials Interfaces*, 2014. **6**: p. 1113-1124.

22. Chen, J. S., C. Chen, J. Liu, R. Xu, S. Z. Qiao and X. W. Lou. *Chemical Communications*, 2011. **47**: p. 2631-2633.

23. Liu, S., N. Zhang, Z. R. Tang and Y. J. Xu. *ACS Applied Materials Interfaces*, 2012. **4**: p. 6378-6385.

24. Wu, W., S. Zhang, F. Ren, X. Xiao, J. Zhou and C. Jiang. *Nanoscale*, 2011. **3**: p. 4676-4684.

25. Bessekhouad, Y., D. Robert and J. V. Weber. *Catalysis Today*, 2005. **101**: p. 315-321.

26. Yang, G., W. Yan, Q. Zhang, S. Shen and S. Ding. *Nanoscale*, 2013. **5**: p. 12432-12439.

27. Xu, X., G. R. Yang, J. Liang, S. J. Ding, C. L. Tang, H. H. Yang, W. Yan, G. D. Yang and D. M. Yu. *Journal of Materials Chemistry A*, 2014. **2**: p. 116-122.

28. Han, Y. T., X. Wu, Y. L. Ma, L. H. Gong, F. Y. Qu and H. J. Fan. *CrystEngComm*, 2011. **13**: p. 3506-3510.

29. Yang, H. Y., S. F. Yu, S. P. Lau, X. Zhang, D. D. Sun and G. Jun. *Small*, 2009. **5**: p. 2260-2264.

30. Yin, Y. X., L. Y. Jiang, L. J. Wan, C. J. Li and Y. G. Guo. *Nanoscale*, 2011. **3**: p. 1802-1806.

31. Chen, J. S., Y. L. Tan, C. M. Li, Y. L. Cheah, D. Luan, S. Madhavi, F. Y. Boey, L. A. Archer and X. W. Lou. *Journal of the American Chemical Society*, 2010. **132**: p. 6124-6130.

32. Yu, J., T. Ma and S. Liu. *Physical Chemistry Chemical Physics*, 2011. **13**: p. 3491-3501.

33. Peng, X. S. and A. C. Chen. *Advanced Functional Materials*, 2006. **16**: p. 1355-1362.

34. Liu, M., L. Piao, L. Zhao, S. Ju, Z. Yan, T. He, C. Zhou and W. Wang. *Chemical Communications*, 2010. **46**: p. 1664-1666.

35. Chen, J. S., Y. L. Tan, C. M. Li, Y. L. Cheah, D. Luan, S. Madhavi, F. Y. C. Boey, L. A. Archer and X. W. Lou. *Journal of the American Chemical Society*, 2010. **132**: p. 6124-6130.

36. Zhang, L., C. Hu, J. Zhang, L. Cheng, Z. Zhai, J. Chen, W. Ding and W. Hou. *Chemical Communications*, 2013. **49**: p. 7507-7509.

37.Zhou, W., C. Cheng, J. Liu, Y. Y. Tay, J. Jiang, X. Jia, J. Zhang, H. Gong, H. H. Hng, T. Yu and H. J. Fan. *Advanced Functional Materials*, 2011. **21**: p. 2439-2445.

38. Zhang, D.-F., L.-D. Sun, C.-J. Jia, Z.-G. Yan, L.-P. You and C.-H. Yan. *Journal of the American Chemical Society*, 2005. **127**: p. 13492-13493.

39. Wang, C., C. Shao, X. Zhang and Y. Liu. *Inorganic Chemistry*, 2009. **48**: p. 7261-7268.

40. Tada, H., A. Hattori, Y. Tokihisa, K. Imai, N. Tohge and S. Ito. *Journal of Physical Chemistry B*, 2000. **104**: p. 4585-4587.

41. Mani, J., H. Sakeek, S. Habouti, M. Dietze and M. Es-Souni. *Catalysis Science & Technology*, 2012. **2**: p. 379-385.

42. Li, D. and Y. Xia. *Advanced Materials*, 2004. **16**: p. 1151-1170.

43. Lee, S. S., H. W. Bai, Z. Y. Liu and D. D. Sun. *Int. J. Hydrogen Energ.*, 2012. **37**: p. 10575-10584.

44. Bandara, J., C. C. Hadapangoda and W. G. Jayasekera. *Applied Catalysis B: Environmental*, 2004. **50**: p. 83-88.

45. Pan, J., M. I. B. Utama, Q. Zhang, X. F. Liu, B. Peng, L. M. Wong, T. C. Sum, S. J. Wang and Q. H. Xiong. *Advanced Materials*, 2012. **24**: p. 4151-4156.

46. Anpo, M. and M. Takeuchi. *Journal of Catalysis*, 2003. **216**: p. 505-516.

47. Zhang, H., X. Lv, Y. Li, Y. Wang and J. Li. *ACS Nano*, 2009. **4**: p. 380-386.

48.Chen, J. I. L., G. von Freymann, S. Y. Choi, V. Kitaev and G. A. Ozin. *Advanced Materials*, 2006.

18: p. 1915-1919.

49. Snaith, H. J., A. J. Moule, C. Klein, K. Meerholz, R. H. Friend and M. Grätzel. *Nano Letter*, 2007. **7**: p. 3372-3376.

50. Li, G., N. M. Dimitrijevic, L. Chen, J. M. Nichols, T. Rajh and K. A. Gray. *Journal of the American Chemical Society*, 2008. **130**: p. 5402-5403.

Figure Captions

Scheme 1 Schematic of the photodegrade mechanism of the SnO_2@TiO_2 porous nanowire-nanosheet heterostructures

Scheme 2 The **s**chematic of the synthetic procedures of SnO_2@TiO_2 porous nanowire-naosheet heterostructures.

Figure 1 TEM images (a) of SnC_2O_4 precursor, (b) porous SnO_2 nanowires, respectively, (c) SEM image and (d, e, f) TEM images of SnO_2@TiO_2 heterostructures.

Figure 2 The formation process of the SnO_2@TiO_2 heterostructures (a,1 h; b, 4 h; c,8 h; d,16 h;)

Figure 3 TEM image of the SnO_2@TiO_2 heterostructures without (a) and with (b) assisted DETA.

Figure 4 XRD patterns of the SnC_2O_4 precursor, SnO_2 porous nanowires and SnO_2@TiO_2 heterostructures.

Figure 5 UV-Vis optical absorption spectra of SnO_2 porous nanowires and SnO_2@TiO_2 heterostructures.

Figure 6 The Degradation plots (a: SnO_2, b: SnO_2@TiO_2), degradation rate of the samples of SnO_2 porous nanowires, SnO_2@TiO_2 nanowire heterostructures and for the degradation of RhB solution urder the irradiation of mixed light (c, d).

Figures

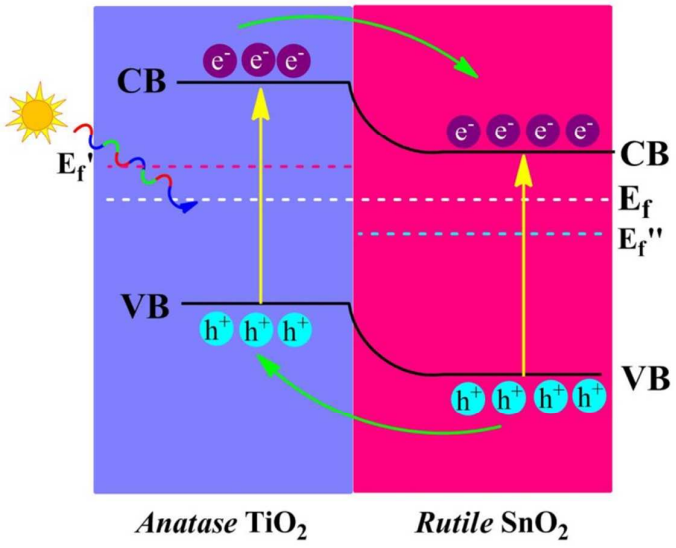

Scheme 1

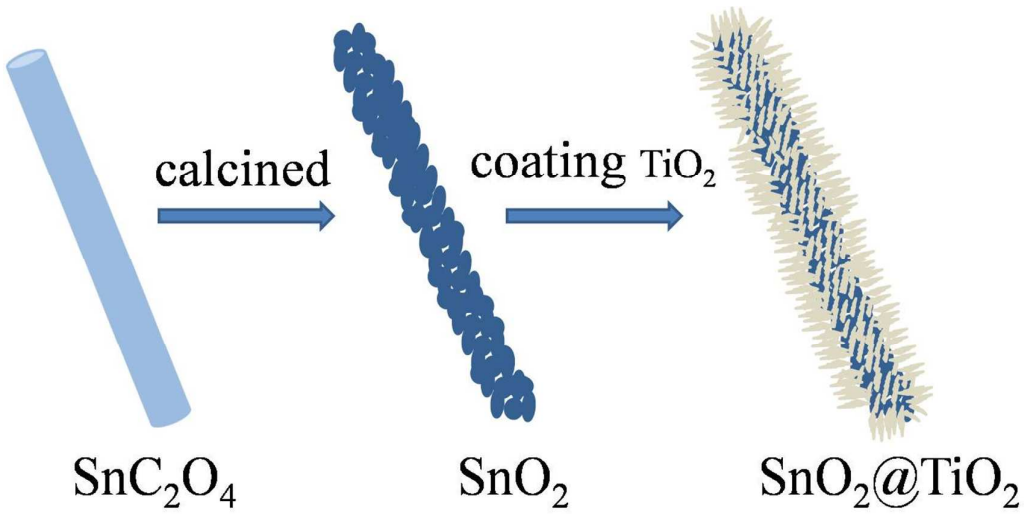

Scheme 2

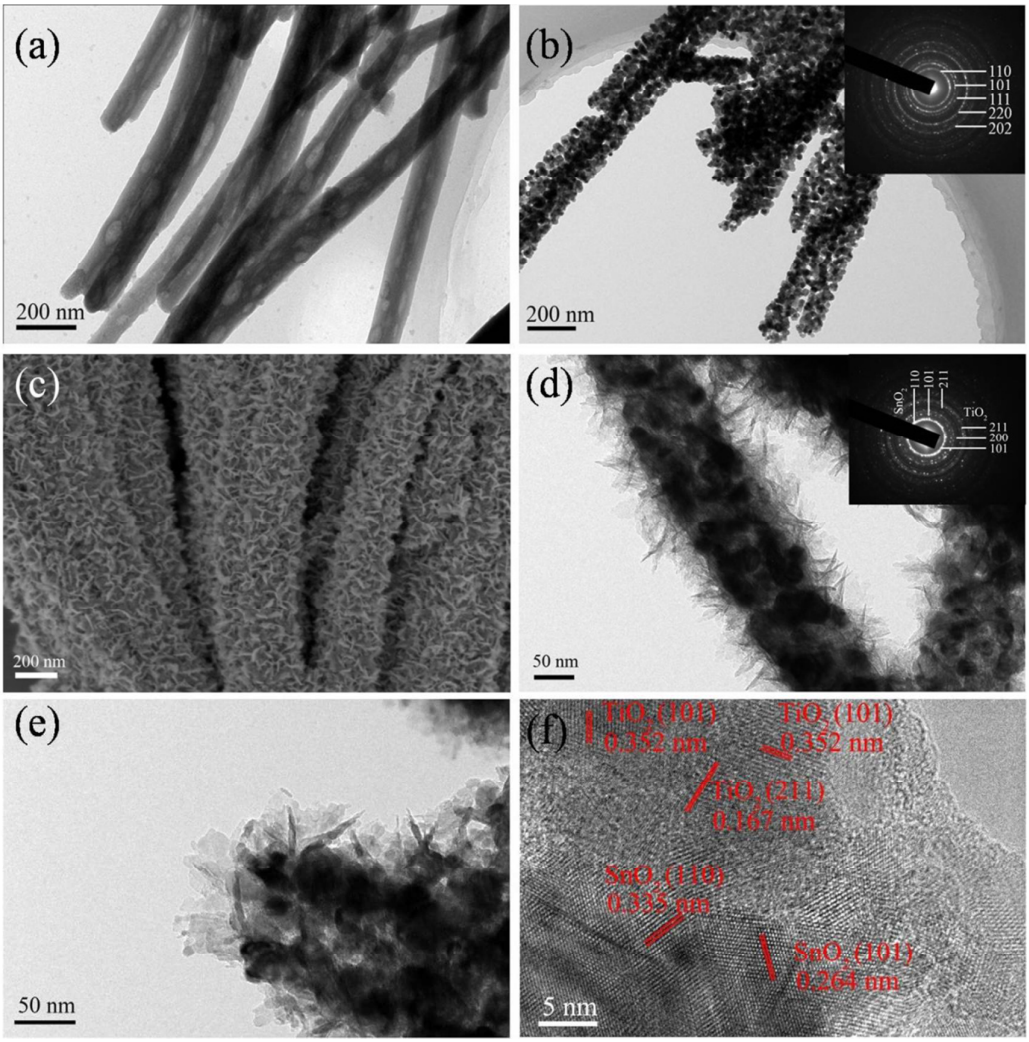

Figure1

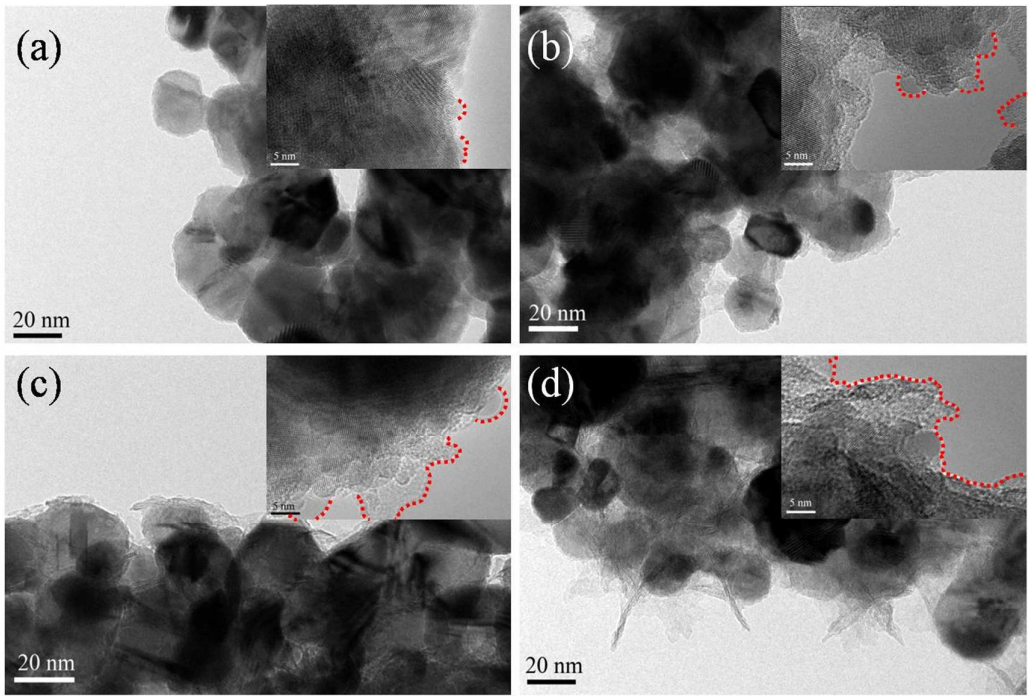

Figure 2

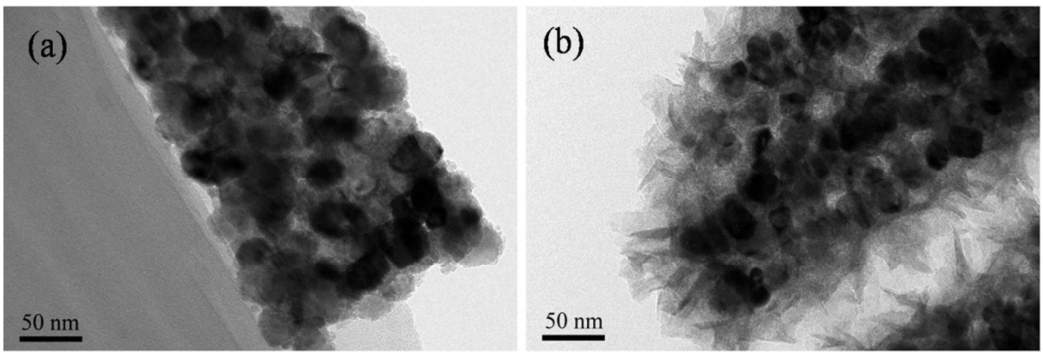

Figure 3

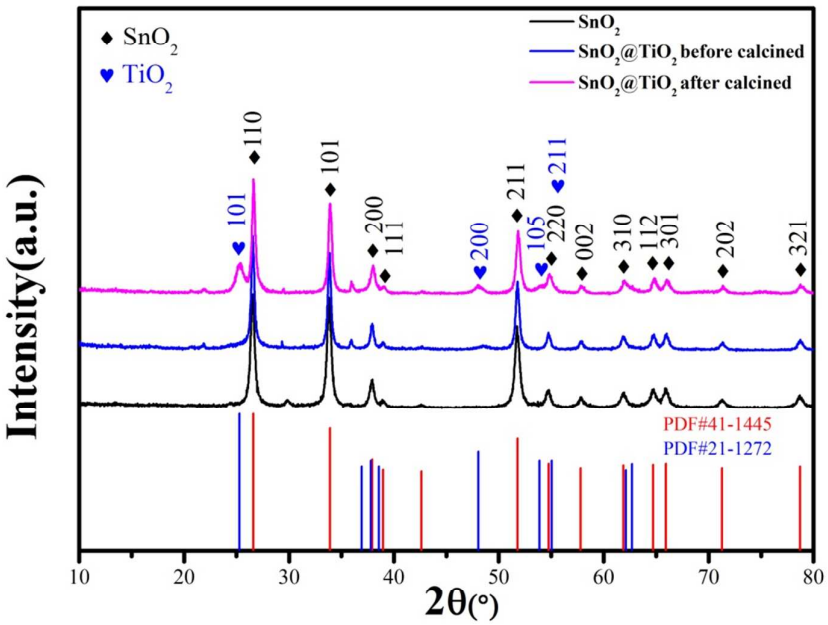

Figure 4

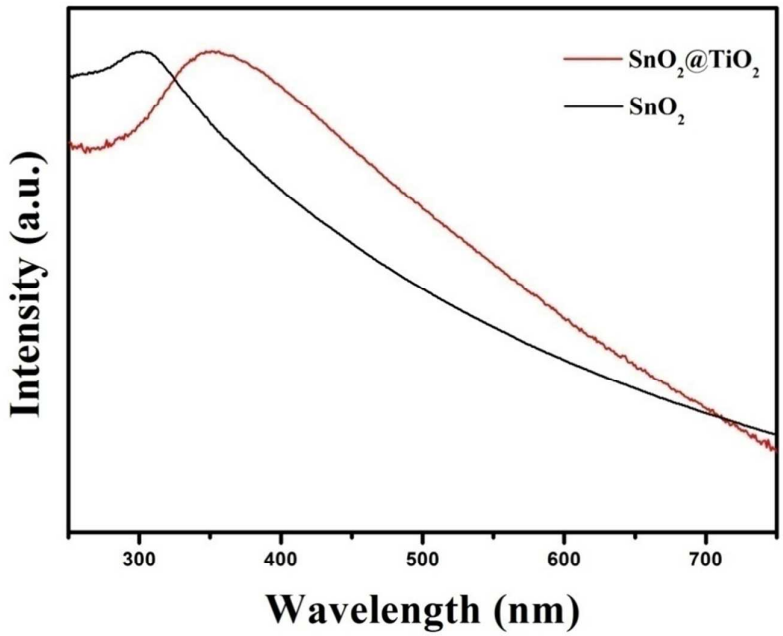

Figure 5

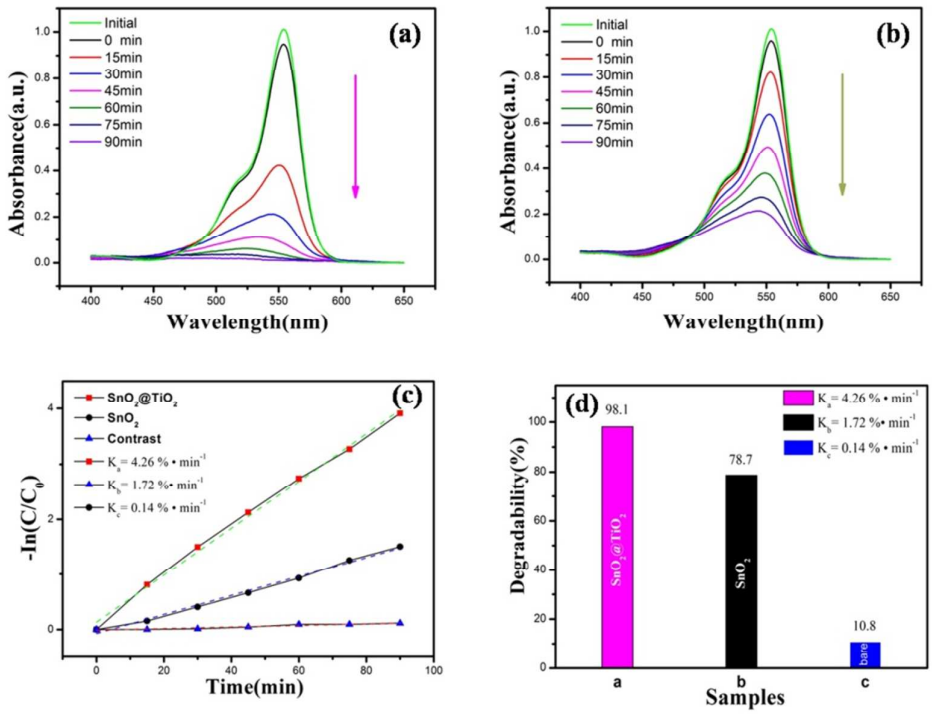

Figure 6

TOC

Self-Assembly SnO_2@TiO_2 Porous Nanowire-Nanosheet Heterostructures for Enhanced Photocatalytic Properties

Banghong Zhou,[1] Shuanglei Yang,[1] Wei Wu,[2] Lingling Sun,[3] Mei Lei,[3] Jun Pan[1,] and Xiang Xiong[1,*]*